Key role of density functional approximation in predicting M-N-C catalyst activities for oxygen reduction

Brett Henderson,[*,†,‡] Sofia Donnecke,[†,‡] Scott N. Genin,[¶] Ilya G. Ryabinkin,[¶] and Irina Paci[†,‡]

†*Department of Chemistry and the Centre for Advanced Materials and Related Technology, University of Victoria, Victoria, British Columbia, V8P 5C2, Canada*

‡*Quantum Algorithms Institute, Surrey, British Columbia, V3T 5X3, Canada*

¶*OTI Lumionics Inc., 100 College St. #351, Toronto, Ontario, M5G 1L5, Canada*

E-mail: bhenderson@uvic.ca

Phone: +1 (760) 807-4785

Abstract

Metal-Nitrogen-Carbon motifs present intriguing structural and electronic properties for a number of applications, including as oxygen reduction catalysts. However, computational investigations of M-N-C-catalyzed reactions have must grapple with their complex electronic structures. In the present study, we evaluate the impact of the density functional approximation on calculated M-N-C catalyst activities for oxygen reduction. Using metalloporphyrins as model catalysts, we find a significant split between pure (GGA) and hybrid functionals, with hybrid functionals, in particular B3LYP, showing greater agreement with DLPNO-CCSD(T) reaction energies. Notably, double-hybrids offered no noticeable improvement over the much more computationally efficient B3LYP and PBE0. Other discrepancies between functionals,

including ground state spin and geometry, are also considered in this work. Finally, both hybrid and double-hybrid functionals greatly reduced the gas phase errors associated with the main group molecules in the oxygen reduction reaction relative to GGA calculations, leading us to question the application of widely used empirical corrections to O_2.

1 Introduction

The oxygen reduction reaction (ORR) is a crucial biological process and a critical component of developing technologies such as metal-air batteries and hydrogen fuel cells. For hydrogen fuel cells, the ORR is current-limiting, and cathodes generally contain platinum catalysts to produce the current needed for industrial applications.[1] The broader commercialization of these devices relies on developing catalysts that are cheap, abundant, and active relative to the current state of the art.

Computational studies aid the design of novel catalysts in part by defining the factors that limit theoretical catalyst activity. Density functional theory has shown that most ORR catalysts are constrained by linear free energy scaling relationships (LFESRs) between the binding energies of reaction intermediates.[2] These scaling relationships can be used to derive characteristic volcano plots that relate catalyst activities to the binding energy of a single ORR intermediate. Such plots show that Pt is near, but not at, the theoretical peak activity of metallic surfaces, and that a significant overpotential will remain unless these LFESRs can be broken or circumvented by a novel class of catalyst.[2] As a result, new catalytic materials are sought to push catalyst activity past typical volcano plot scaling and provide alternatives to Pt.[3–5]

Porphyrins and M-N-C sites more generally have attracted considerable attention as non-platinum group ORR catalysts with high theoretical limiting potentials[2] and experimentally demonstrated activities competitive with Pt-based catalysts.[6] Because of the tunability of functional groups on these porphyrins, their activity and selectivity toward either the two-electron or four-electron ORR can also be optimized,[7,8] making them promising scaffolds on which to build next generation ORR catalysts. A cycle depicting possible mechanisms for both of these pathways on a metal porphyrin

catalyst is shown in Figure 1. Furthermore, bifunctional materials based on porphyrins are expected to break typical scaling relationships through differentiating interactions between adsorbed intermediates and nearby functional groups, which can preferentially stabilize the OOH intermediate.[4,5]

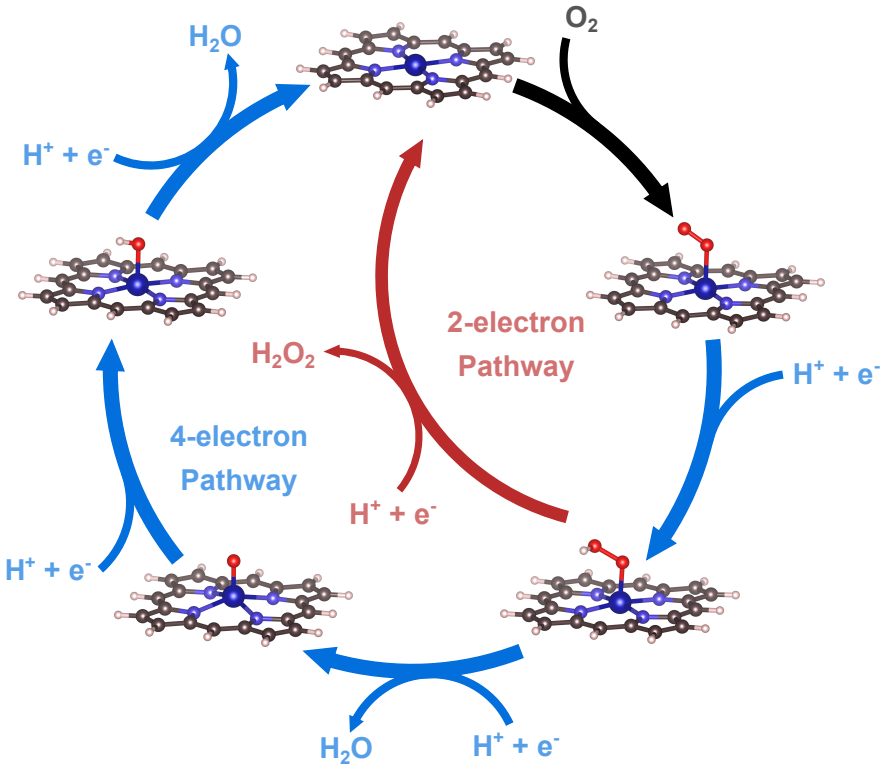

Figure 1: Catalytic cycle for oxygen reduction on a metal porphyrin catalyst. Outer loop shows the associative 4-electron pathway studied herein, while the inner loop shows the 2-electron pathway producing H_2O_2.

Despite their promise, describing the electronic structure of transition metal porphyrins is no trivial endeavor. These molecules possess complicated electronic structures which make the determination of ground spin states[9] and binding energies[10,11] challenging and highly dependent on the particular density functional approximation employed.[10,12] Studies aimed at related molecules have indicated that single hybrid functionals with small amounts of Hartree-Fock exchange perform well relative to wavefunction theories[12,13] and experiment.[5] The recommendation of these functionals also agrees with generalized benchmarking efforts on transition metal complexes[14–16] (an overview of these works is provided in Table S1).

In the present work, we aim to understand the impact of density functional on the predicted ORR activity of 3d-metalloporphyrin catalysts. We calculate scaling relationships and theoretical overpotentials using six popular functionals that span different levels of approximation and compare results against the efficient coupled cluster variant DLPNO-CCSD(T) (Domain-Based Local Pair Natural Orbital Coupled Cluster with explicit Singles and Doubles excitations and a perturbative Triples correction). In doing so, we expand upon the work in Ref 12 by using large basis sets and dispersion corrections throughout, investigating the double-hybrid B2PLYP, and focusing on metals relevant for the ORR (including iron porphyrins). In addition, we scrutinize the sources of discrepancy between the functionals considered here, including the identification of ground spin states, geometry optimizations, and empirical gas-phase corrections.

2 Methods

2.1 Model Catalysts

We investigate four metalloporphyrin (MP) catalysts containing manganese (MnP), iron (FeP), cobalt (CoP) and nickel (NiP). Manganese, iron, and cobalt porphyrins, including functionalized variants, have been explored extensively for the ORR.[4,5,7,17–20] Nickel porphyrin has received only minimal attention as ORR catalysts due to its weak binding of O_2,[7,21] yet its inclusion herein is useful as a way to cover the weak binding regime in the construction of LFESRs. Since MPs closely resemble pyrrolic MN_4 catalytic sites in M-N-C catalysts, we expect the conclusions drawn about the performance of different functionals to be relevant for this broader class of catalysts. Thus, the MPs considered herein comprise a valuable test set because they represent a class of notoriously complicated but widely studied 3d complexes spanning a range of ORR activities.

2.2 Reaction Mechanism

The ORR catalytic activity of metalloporphyrins was assessed for the 4-electron associative pathway depicted in Figure 1 and in the reaction scheme in eqs 1(a)-(e). The reaction proceeds through the intermediate complexes $MP(O_2)$, MP(OOH), MP(O), MP(OH). It is worth noting that many ORR studies neglect the initial step of this pathway, the binding of O_2 to the catalyst. However, we have included this step because 1) it shows a large dependence on functional choice, 2) there is ample experimental and computational data on this step available for comparison, and 3) the oxygen binding geometry and energetics are correlated with molecular catalyst activity for the ORR.[17,22] As the goal of this work is to assess the variability and accuracy of various functionals, the porphyrins themselves were kept unfunctionalized. This minimized the computational complexity and facilitated the use of high accuracy single-reference methods.

$$\mathrm{MP} + \mathrm{O_2} \longrightarrow \mathrm{MP(O_2)} \tag{1a}$$

$$\mathrm{MP(O_2)} + \mathrm{H^+} + \mathrm{e^-} \longrightarrow \mathrm{MP(OOH)} \tag{1b}$$

$$\mathrm{MP(OOH)} + \mathrm{H^+} + \mathrm{e^-} \longrightarrow \mathrm{MP(O)} + \mathrm{H_2O} \tag{1c}$$

$$\mathrm{MP(O)} + \mathrm{H^+} + \mathrm{e^-} \longrightarrow \mathrm{MP(OH)} \tag{1d}$$

$$\mathrm{MP(OH)} + \mathrm{H^+} + \mathrm{e^-} \longrightarrow \mathrm{MP} + \mathrm{H_2O} \tag{1e}$$

2.3 Computational Hydrogen Electrode

The ORR was studied using the Computational Hydrogen Electrode (CHE).[23] Free energies were calculated using the electronic energy (E_{el}), zero-point energy (ZPE), heat capacity corrections to the internal energy (E_{therm}), entropic effects ($-TS$), and solvation effects (E_{solv}):

$$G = E_{\mathrm{el}} + ZPE + E_{\mathrm{therm}} - TS + E_{\mathrm{solv}} \tag{2}$$

For a given set of reaction intermediates, the free energy at electrode potential U was shifted by

$-neU$, where n is the number of proton-electron pairs present in the reactants of a given step of the balanced reaction, and e is the charge of an electron. All calculations correspond to pH = 0, and electric field effects were ignored.

Solvation Corrections. In this work, ΔE_{solv} is modeled by a solvation correction of -0.30 eV applied to the free energy of the MP(OH) and MP(OOH) intermediates, as implemented in previous works.[7,24,25] Recent benchmarking has shown that such a correction may underestimate the solvation energy of the MP(O) intermediate for single-atom catalysts relative to implicit and explicit solvent models.[13,26] Nevertheless, the use of a simple, functional-independent solvent model eliminates the need to validate implicit or explicit solvation models, while allowing comparison to earlier studies using the correction.

Thermodynamic Corrections. Thermal and entropic corrections were evaluated at 298.15 K. The pressure for entropic corrections was taken to be 1 bar, except for the calculation of H_2O, which used a pressure of 0.035 bar. At this pressure, liquid and gaseous water are in equilibrium, allowing the free energy of the calculated gaseous water to be equated to that of liquid water as defined in the ORR half cell reaction.[23,27,28]

Empirical O_2 Correction. The free energy of O_2 was set such that the overall reaction free energy of the 4-electron pathway would match the theoretical value of 4.92 eV,[29,30] as is standard practice in ORR studies.[23,28]

Theoretical Overpotentials. Theoretical overpotentials were calculated as the difference between the theoretical half-cell potential for ORR (1.23 V) and the highest potential at which all steps in the free-energy pathway remained downhill.[23] For these calculations, binding of dioxygen (1(a)) was not considered. Instead, steps 1(a) and (b) were considered a single step, as is customary in the CHE.

Energies for Linear Scaling Relationships. The energies of intermediate species were also calculated relative to the product energies following the convention of Nørskov *et al.*[23] Specifically, the relative free energies ΔG_{OOH}, ΔG_{O}, and ΔG_{OH} are calculated as the free energy changes of the following reactions, respectively:

$$\mathrm{MP} + 2\mathrm{H_2O} \longrightarrow \mathrm{MP(OOH)} + \frac{3}{2}\mathrm{H_2} \tag{3}$$

$$\mathrm{MP} + \mathrm{H_2O} \longrightarrow \mathrm{MP(O)} + \mathrm{H_2} \tag{4}$$

$$\mathrm{MP} + \mathrm{H_2O} \longrightarrow \mathrm{MP(OH)} + \frac{1}{2}\mathrm{H_2} \tag{5}$$

Where only the electronic energies are considered, these relative energies are referred to as ΔE_{OOH}, ΔE_{O}, and ΔE_{OH}.

2.4 Computational Details

All calculations were performed using ORCA 5.0.4.

DFT Calculation Details. The seven exchange-correlation functionals employed in the present study are described in Table 1. Grimme's D3 dispersion correction with Becke-Johnson damping parameters [D3(BJ)] was applied to all functionals.[31,32] The chosen functionals encompass a range of theoretical approximations, from pure GGA to double-hybrid GGA. As the trends observed in the present study often coincide with the unofficial rungs of Jacob's ladder proposed by Perdew,[33] we include them for ease of classification in the later discussion.

Table 1: Overview of the functionals used.

Functional	Class[a]	Rung[b]	%EXX[c]	%MP2[d]	Ref.
BP86	GGA	2	–	–	34,35
PBE	GGA	2	–	–	36
TPSSh	Hybrid Meta-GGA	4	10	–	37
B3LYP	Hybrid GGA	4	20	–	38
PBE0	Hybrid GGA	4	25	–	39
B2PLYP	DH GGA	5	53	27	40
PWPB95	SOS DH Meta-GGA	5	50	27	41

[a] DH = Double-Hybrid. SOS = Spin-Opposite Scaled.
[b] Rung on the informal Jacob's ladder categorization of functionals.[33]
[c] Percentage of exact exchange included in the functional.
[d] Percentage of MP2 correlation included in the functional.

All structures were optimized using the def2-TZVP basis set using each of the first six functionals in Table 1. After optimization, single point calculations were performed using the def2-QZVPP basis set. Stability analysis was performed on the wavefunctions,[42] and where necessary, the calculations were restarted using rotated orbitals until stability was achieved.

In some cases, B2PLYP optimizations showed signs of instability, never reaching the force thresholds required for convergence. When the energies seemed sufficiently converged to make an assessment of ground state spin and geometry, the lowest energy structure along the optimization path was selected. These unconverged structures are indicated in the Table S7. Because frequency calculations could not be performed on geometries that were not fully converged, B2PLYP was omitted from the construction of LFESRs and volcano plots.

For each complex, low-, intermediate-, and high-spin structures were optimized, and the ground state spin was determined independently for each functional from the lowest single-point electronic energy of the three tested spin states. The full list of DFT-predicted multiplicities is given in Table S5. In general, these did not agree between functionals. Thus, the true ground state multiplicity for each intermediate was assigned using reference values from experiment or high-level wavefunction theory when available, or the lowest-energy state from our own DLPNO-CCSD(T) calculations otherwise. Neither of these options were available for NiP(O_2), but all tested functionals predicted a triplet ground state, which we assumed to be accurate.

DLPNO-CCSD(T) Calculations. DLPNO-CCSD(T) calculations were performed on TPSSh-optimized geometries, using TPSSh reference orbitals. The iterative triples correction of Guo *et al.*[43] was employed, as it yields better relative energies for transition metal systems and other molecules with low-lying excited states.[44] Due to the large disk-space demands of this procedure, the cutoff for including triple natural orbitals (TCutTNO) was increased from 1.0×10^{-9} to 5.0×10^{-9}. This allowed all calculations to be performed on 2 TB of local disk space. Benchmarking illustrated that this change had minimal effect on the accuracy of the method (Section S2), which is consistent with earlier benchmarking done by Guo *et al.*[44]

For calculations of ΔE_O and ΔE_{OH}, and ΔE_{OOH} two-point complete basis set (CBS) extrap-

olation was performed using the aug-cc-pvdz and aug-cc-pvtz basis sets on all atoms using the procedure and fitting parameters of Neese and Valeev.[45] In addition, an extrapolation to the complete pair natural orbital space (CPS)[46] was performed using the CPS1 variant procedure described by Drosou *et al.*, which was shown to greatly improve spin-splitting energies in iron complexes.[9] In all cases, the NormalPNO setting was employed, though the TCutPNO setting was modified for the CPS extrapolation. For calculating the lowest energy spin states, the same CBS/CPS procedure was used. However, only the basis set of the metal atom was extrapolated, which improved efficiency while accurately treating the orbitals important for determining multiplicity. These calculations used the following basis sets: def2-SVP for H and C, def2-TZVP for N and O, and def2-TZVPP / def2-QZVPP for the metal.

CCSD(T) Calculations. CCSD(T) calculations were performed on H_2O, O_2, and H_2 as well as atomic O and H in order to benchmark density functional performance for the overall oxygen reduction reaction. All calculations used B2PLYP geometries, a UHF reference, and a cc-pv6z basis. For free energy evaluations, the ZPE, thermal, and entropic corrections were taken from B2PLYP calculations.

3 Results and Discussion

3.1 Linear Free Energy Scaling Relationships

LFESRs were found to exhibit significant dependence on the choice of functional, which impacts the derived volcano plots of catalyst activity. Figure 2 depicts the LFESRs between MP(O) and MP(OH) [Figure 2(a)] and MP(OOH) and MP(OH) [Figure 2(b)], calculated using all GGA and single-hybrid functionals.

The fitted scaling relationships depicted in Figure 2(a) and (b) show a monotonic decrease in slope and increase in intercept as the percentage of exact exchange in the functional increases (see Table 1). Thus, the fits for BP86 and PBE, which contain no exact exchange, are quite similar. Among the hybrid functionals, TPSSh shows the closest agreement with the pure GGAs, likely

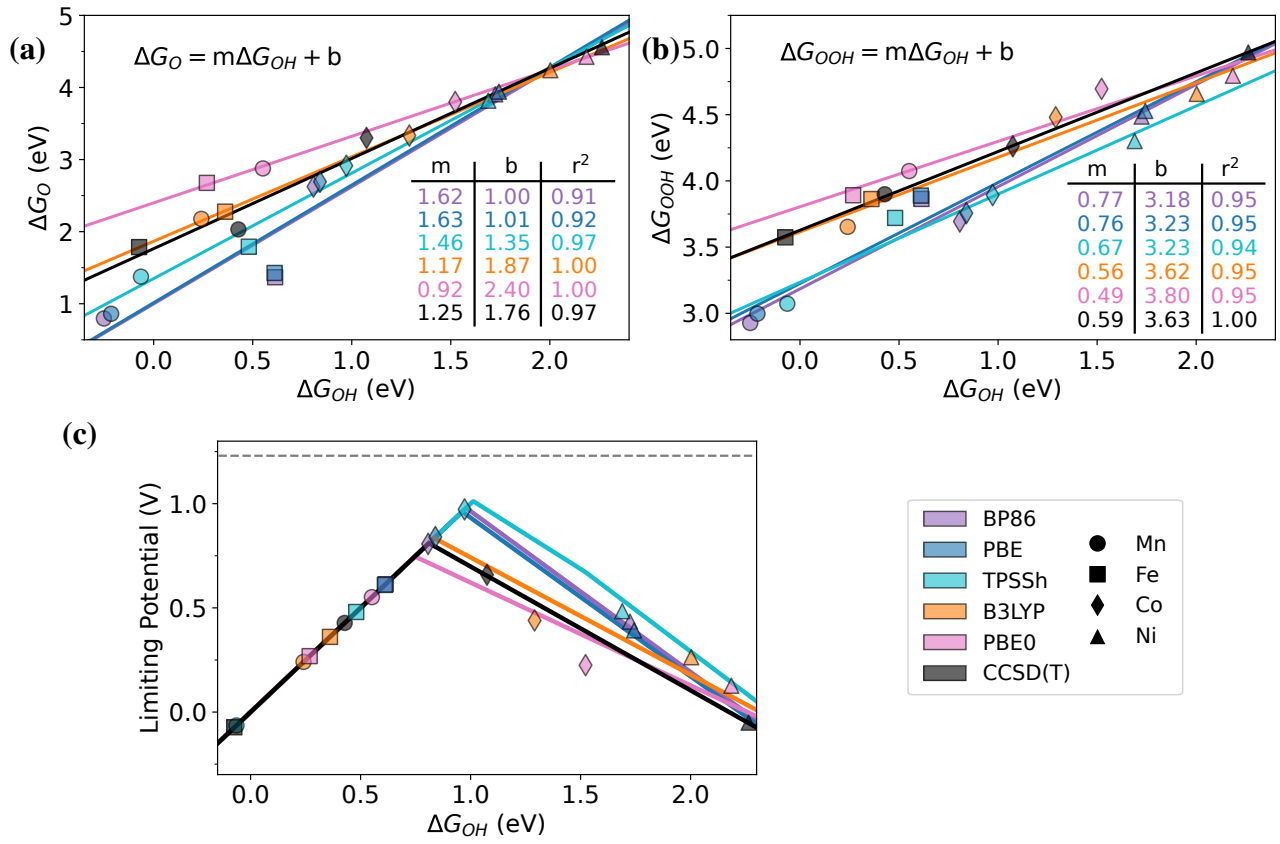

Figure 2: Dependence of theoretical catalyst activity on employed density functional. Linear free energy scaling relationships between the binding energies of **(a)** MP(O) and MP(OH) and **(b)** MP(OOH) and MP(OH). Parameters and r^2 values for the fit lines are shown as insets. Note that the different scale in **(b)** indicates a narrower range of energies for ΔG_{OOH}. **(c)** shows the resulting volcano plots derived from these scaling relationships. The theoretical ORR potential (1.23 V) is depicted as a dashed line above the volcano apex.

owing to its small amount of exact exchange. In contrast, the low slopes of the fits for B3LYP and PBE0 indicate significantly weaker binding of the OOH and O intermediates compared to the GGA predictions. This dependence on exact exchange is quite similar to that found by Busch et al. in the context of the water oxidation reaction on perfluoroporphyrins.[12] Finally, LFESRs constructed using BP86-optimized geometries and free energy corrections (Figure S2) display the same trends and show that B2PLYP produces very similar fit lines to PBE0.

Based on electron-counting rules devised from adsorption on metal surfaces, one would expect the slope of the O/OH and OOH/OH LFESRs to be 2 and 1, respectively.[47] All functionals deviate significantly from this expectation. For GGA functionals, this discrepancy is likely caused by

the lack of a flexible solvent model.[26] However, the much larger deviation for hybrid functionals cannot be dismissed so easily—indeed, such low slopes for the O/OH LFESR were seen to persist even under the application of an implicit solvent model in Ref 12. Therefore, hybrid functionals, in particular those with greater than 10% exact exchange, do not support the commonly accepted assumption that the O ligand forms a double bond to the catalyst, whereas the OOH and OH ligands form single bonds.[2,47] Instead, these functionals predict that the M–O and M–OH bonds are rather similar in nature (this is reflected in the near-unity slope of the scaling relationship shown in Figure 2(a)), and that the M–OOH bond is weaker than the M–OH bond by about half (Figure 2(b)).

Combined, these effects mean that the hybrid functionals (other than TPSSh) predict a significantly less optimistic volcano plot than GGAs (Figure 2(c)), with minimum overpotentials of 0.39 V and 0.51 V for B3LYP and PBE0, respectively. Furthermore, the volcano plot is less symmetrical for these functionals. The right leg, corresponding to weak binding of OOH, is limiting for a broader range of OH binding strengths when using B3LYP and PBE0.

DLPNO-CCSD(T) electronic energies were corrected with TPSSh free energy terms to add reference lines to Figure 2. Fitted DLPNO-CCSD(T) LFESRs show remarkable agreement with B3LYP, even though individual data points do not show such a close accord between the two methods. The low slope of the O/OH scaling relation for DLPNO-CCSD(T) shows that PBE and BP86 cannot properly describe the relationship between these two intermediates. However, hybrid functionals do not universally remedy this situation, either, since there is a large variation in slope depending on the particular functional used. B3LYP seems to offer a fortuitous balance between TPSSh and PBE0, which seems to be linked to its intermediate proportion of exact exchange.

It should be noted that these LFESRs were calculated from only four catalysts per functional. Therefore, the coefficients of the best-fit lines should not be relied on as ironclad quantitative relationships. Nevertheless, the sampled MPs encompass a broad range of ΔG_{OH} values that are relevant to ORR, and the linear relationships show good fits to the data. Thus, the trends that emerge between functionals, which correlate well with the amount of exact exchange included in those functionals, represent real differences between functional predictions and not the effects of

noise.

3.2 Benchmarking Relative Energies Against DLPNO-CCSD(T)

To determine which functional predicts the most accurate relative energies for constructing LFESRs, we calculated ΔE_O, ΔE_{OH}, and ΔE_{OOH} using DLPNO-CCSD(T) and compared against the DFT values. Due to the expense of computing vibrational energies with DLPNO-CCSD(T), only electronic energies are presented in Figure 3. Unlike the LFESRs above, TPSSh/def2-TZVP geometries were used for all DFT and DLPNO-CCSD(T) single point calculations. An additional double-hybrid functional, the spin-opposite scaled PWPB95, which has performed well in recent benchmarking of transition metal reaction energies,,[16,48] was also included for comparison with B2PLYP.

As shown in Figure 3, BP86 and PBE significantly underestimate ΔE_O ΔE_{OH}, and ΔE_{OOH} relative to DLPNO-CCSD(T), indicating overbinding of intermediates [FeP(OH) is the notable exception in panel (b)]. TPSSh behaves similarly, albeit with a slightly lower Mean Absolute Error (MAE). In contrast, PBE0, B2PLYP, and PWPB95 have lower MAEs but generally exhibit slight underbinding, summarized by their positive Mean Signed Errors (MSEs) for all intermediates in Figure 3(d). B3LYP falls between these two extremes, showing the lowest MAE across all functionals and a small MSE that points to minimal bias toward over- or underbinding. These results further reinforce the observation that increasing the proportion of exact exchange reduces the calculated binding strength of intermediates, with B3LYP striking the proper balance of exact exchange. They also indicate that while hybrid functionals offer a significant improvement over GGAs, there appears to be no benefit to using double-hybrid functionals.

MAEs across the three intermediates indicate that the bound O atom is treated less accurately than bound OH and OOH for nearly all functionals, but especially so for the GGA and double-hybrid functionals. GGAs are believed to provide a less accurate treatment of O-O double bonds than single,[49] and it is possible that a similar effect is at play with the formally double-bound O atom here. The poor performance of B2PLYP and PWPB95 for O is somewhat surprising

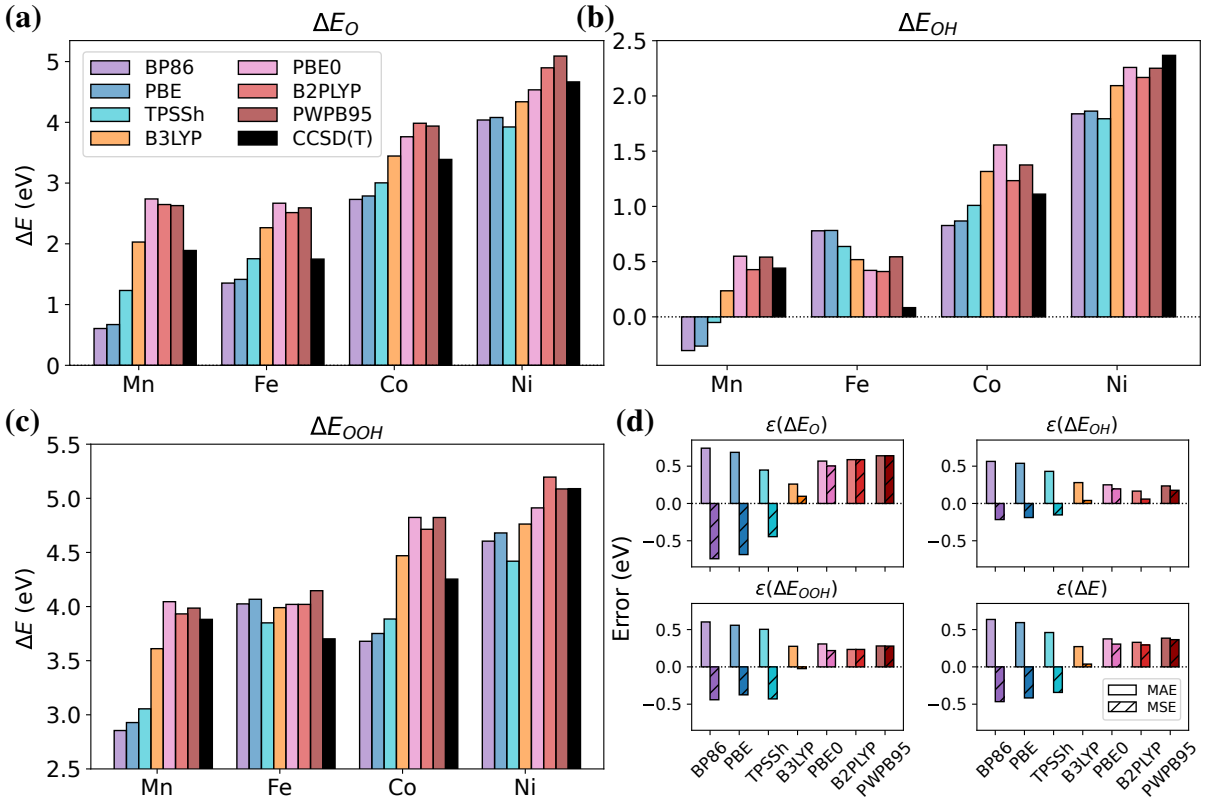

Figure 3: Benchmarking of relative energies of intermediates against DLPNO-CCSD(T). Panels **(a)**, **(b)**, and **(c)** show the relative energies of the bound O, OH, and OOH ligands, respectively. The plots in panel **(d)** show the Mean Absolute Error (MAE) and Mean Signed Error (MSE) of each functional relative to DLPNO-CCSD(T) for each of these ligands as well as the combined errors across all ligands ($\varepsilon(\Delta E)$).

considering how well they perform on the other intermediates. It is likely that some of the difficulty stems from significant spin contamination in three of the four MP(O) complexes (Figures S3 and S4), which is known to degrade the results of MP2.[50] Interestingly, neither TPSSh nor B3LYP appear to suffer for MP(O), instead showing consistent accuracy across all intermediates.

3.3 Variation in Predicted Spin States

The correct prediction of the ground state spin multiplicities in the present study was an important problem that showed a large dependence on the chosen functional. At a fundamental level, the assignment of the correct ground state can provide mechanistic insights and even guide catalyst design to stabilize specific states with the desired reactivities. When experimental data are lacking,

the spin multiplicities are often assumed from previous computational works, inferred based on theoretical arguments, or even calculated during geometry optimizations at lower levels of theory. Using an inappropriate spin state from one of these sources forces the reaction pathway through an excited state with an associated energetic penalty. Furthermore, the 3d transition metal porphyrins under study are known to contain low-lying excited states associated with both unoccupied metal and porphyrin orbitals, which make the proper determination of ground states challenging for DFT. Complicating the matter, different functionals tend to favor different spin states, albeit in a somewhat predictable way. In particular, including exact exchange in a functional preferentially stabilizes high-spin states in direct proportion to the percentage of exchange included.[51–53] Figure S6 confirms this trend for our systems and demonstrates that the effect is dampened by MP2 contributions in B2PLYP.

Table 2: Ground state multiplicities for metalloporphyrin intermediates.

Metal	Ligand	DFT[a]	CCSD(T)[b]	GS[c]	Ref.	Metal	Ligand	DFT[a]	CCSD(T)[b]	GS[c]	Ref.
Mn	–	6	6	6	6[d]	Co	–	2	2	2	2[d]
Mn	O_2	6	–	4	4[d,e]	Co	O_2	2	–	2	2[d]
Mn	OOH	5	5	5	–	Co	OOH	1	1	1	–
Mn	O	4	2[f]	2	–	Co	O	4	4	4	–
Mn	OH	5	5	5	–	Co	OH	1	1	1	–
Fe	–	3	5	3	3[d]	Ni	–	1	1	1	1[d]
Fe	O_2	1	–	1	1[d,e]	Ni	O_2	3	–	3	–
Fe	OOH	6	6	6	–	Ni	OOH	2	2	2	–
Fe	O	3	3	3	–	Ni	O	5	5	5	–
Fe	OH	6	6	6	6[e]	Ni	OH	2	2	2	–

[a] The most common spin predicted by the functionals studied (excluding PWPB95). Ties granted to the higher multiplicity.
[b] DLPNO-CCSD(T).
[c] Final assignment of the ground state multiplicity in the present work.
[d] Experimental. See Refs. 54,55 for MnP, Ref. 56 for FeP, Ref. 57 for CoP, Refs. 58–60 for NiP, Refs. 61,62 for $MnP(O_2)$, Refs. 63,64 for $FeP(O_2)$, Ref. 65 for $CoP(O_2)$.
[e] High-level wavefunction theory. Ref. 11 for $MnP(O_2)$ and $FeP(O_2)$, Refs. 9,66,67 for FeP(OH).
[f] Splitting energy relative to quartet is less than 1 kcal/mol.

Table 2 shows the ground state multiplicities that we determined by DFT and DLPNO-CCSD(T) alongside those given by experiments and higher level calculations when available. At first glance,

the DFT multiplicities, which were determined by taking the mode of the multiplicities predicted by all functionals, show excellent agreement with DLPNO-CCSD(T) and experimental results. However, this agreement belies the variability amongst the functionals. We compared the spin predictions of each functional against available reference data and our DLPNO-CCSD(T) results (Figure 4(b)). Aside from the marginally best-performing B3LYP (17/20) and worst-performing B2PLYP (15/20), all functionals correctly predicted multiplicities for 16 of the 20 species. However, the erroneous species generally differed from functional to functional, and there was no obvious benefit from moving up rungs of Jacob's ladder. As a result, B2PLYP predicts different ground state spins than any of BP86, PBE, and TPSSh for a concerning 9 out of the 20 studied complexes (Figure S6). Disagreements between functionals do appear to be tied strongly to the impact of exact exchange, with the functional with a higher proportion of exact exchange almost always predicting the higher multiplicity.

Table 2 also highlights in red what we might call poorly behaved intermediates, ones for which at least one functional misassigned the ground state spin. These intermediates tended to be concentrated in the earlier transition metal porphyrins, which exhibit strong binding of oxygen species (note more instances of disagreement in Mn and Fe than for Co and Ni). Cross-referencing with Figure 4(b), we see that pure GGAs and TPSSh tended to excel in determining spin ordering for weak-binding complexes (both later transition metal species and dioxygen species across all metals), while hybrid and double-hybrids improved predictions for stronger-binding complexes at the expense of some accuracy for the late transition metals.

It is important to note that despite the inconsistency among functionals, the DFT spin assignments for nine out of the eleven poorly behaved complexes were reconciled with available reference and DLPNO-CCSD(T) results simply by choosing the most commonly predicted multiplicity. The two exceptions were MnP(O_2), a notoriously challenging system with a low-lying sextet, and MnP(O), which DLPNO-CCSD(T) predicts to have a quartet less than 1 kcal/mol higher than the ground state doublet. For both of these systems, the six tested functionals were evenly split in their spin assignments, which highlights the difficulty that the Mn porphyrins pose for spin state

ordering. Overall, these results show that outside of some exceptional cases, application of several functionals with a range of exact exchange can be a viable approach to determine ground state spins for metalloporphyrins when experimental data or higher-level calculations are unavailable or unfeasible.

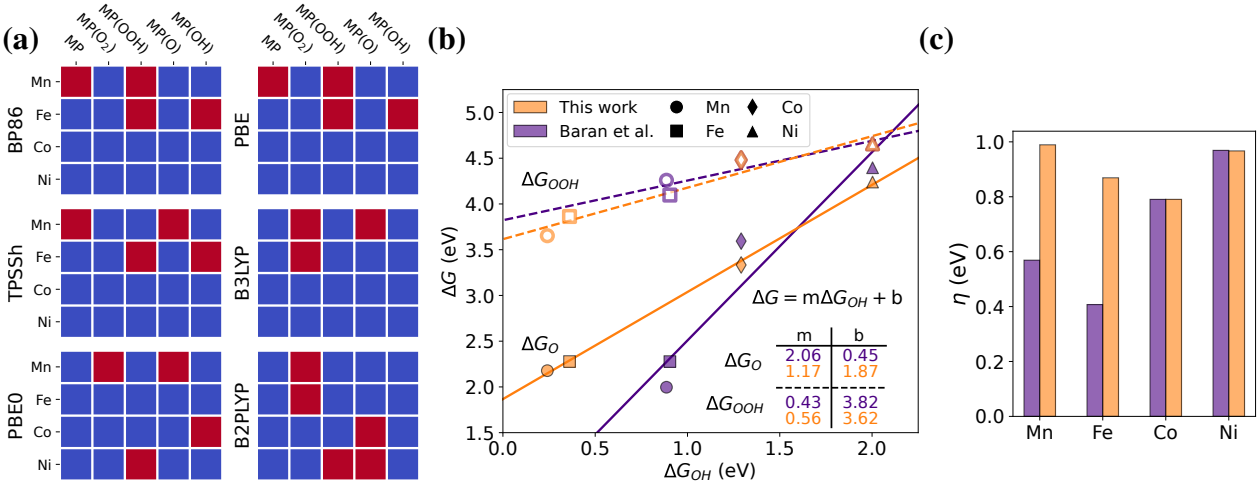

Figure 4: Dependence of ground state spin on employed density functional. **(a)** The correspondence between the GS spin predictions of each functional and the best guess for the true GS spin for each geometry. Blue and red indicate correct and incorrect prediction, respectively. **(b)** The OOH/OH and O/OH LFESRs calculated using B3LYP using either the ground state multiplicities from Ref 7 or from the present study. **(c)** The theoretical overpotentials calculated from these two sets of multiplicities using B3LYP.

Since the difficulty of ground state spin ordering arises largely because these systems have small spin splitting energies, one might assume that the energetic consequences of misassigning the ground state multiplicity would be rather small. Within our data set, when a functional incorrectly predicted the ground state, the true ground state was only 5.4 kcal/mol higher in energy than the incorrect state, on average (median 3.9 kcal/mol). To properly assess the impact of these spin splitting energies, we recalculated the LFESR for the best-performing B3LYP using the ground state spins determined by Baran *et al.* in a previous study using the pure GGA OLYP (See Table S6).[7] Figure 4(b) shows that the O/OH scaling relation was most significantly affected, with the change driven primarily by changes in ΔG_{OH} for MnP and FeP. Recalculated overpotentials in Figure 4(c) tell a similar story, with the overpotentials for MnP and FeP dropping erroneously

by roughly 0.4 eV while the remaining species are largely unchanged. Thus, while the average spin splitting energies for the metalloporphyrins are quite small, it only takes the reversal of spin ordering (or the use of an erroneous ground state spin calculated at a lower level theory) for a single larger gap intermediate to greatly impact theoretical overpotentials.

3.4 Variation in Predicted Geometries

Unlike spin state ordering, structural parameters are often assumed to be relatively insensitive to functional. We found that this assumption held true in general for metalloporphyrins but note some quite substantial outliers. Most notably, as has already been studied for FeP,[10,68] metal-oxygen bond lengths were found to vary directly and strongly with the amount of exact exchange in a functional for the dioxygen adducts of all but the most strongly binding MnP (Figure 5(a) and (c)). A similar variation presented in the very weakly bound NiP(OOH), with GGA functionals preferring a configuration with an outward-facing hydrogen and the remaining functionals predicting hydrogen bond donation to the porphyrin nitrogen (Figure 5(d). Finally, the MP(O) intermediates showed moderate variations of about 0.1 $\AA$ depending on the functional used. On the whole, M–O bondlengths tend to correlate well within rungs of Jacob's ladder (Figure 5(b), even though most intermediates involved in electrocatalysis were fairly robust to changes in functional. Functional type and amount of exact exchange also correlated well with the amount that metal atoms were displaced from the porphyrin plane (Figure S10) but less so with other geometrical parameters like metal-nitrogen bond lengths and the degree of ruffling and saddling of the macrocycle (Figures S9, and S11).

A natural question is whether the level of theory used for geometry optimization really matters energetically, for instance when computing catalyst activities. Figure 6(b) quantifies the energetic difference between each geometry optimized at the BP86 level and the energy of the re-optimized geometry for each other functional we tested. These relative energies are plotted against the RMSD for BP86 and re-optimized geometries as described in Figure 6(a) to understand how sensitive these systems are to small structural changes. For the most part, the structural and energetic differences

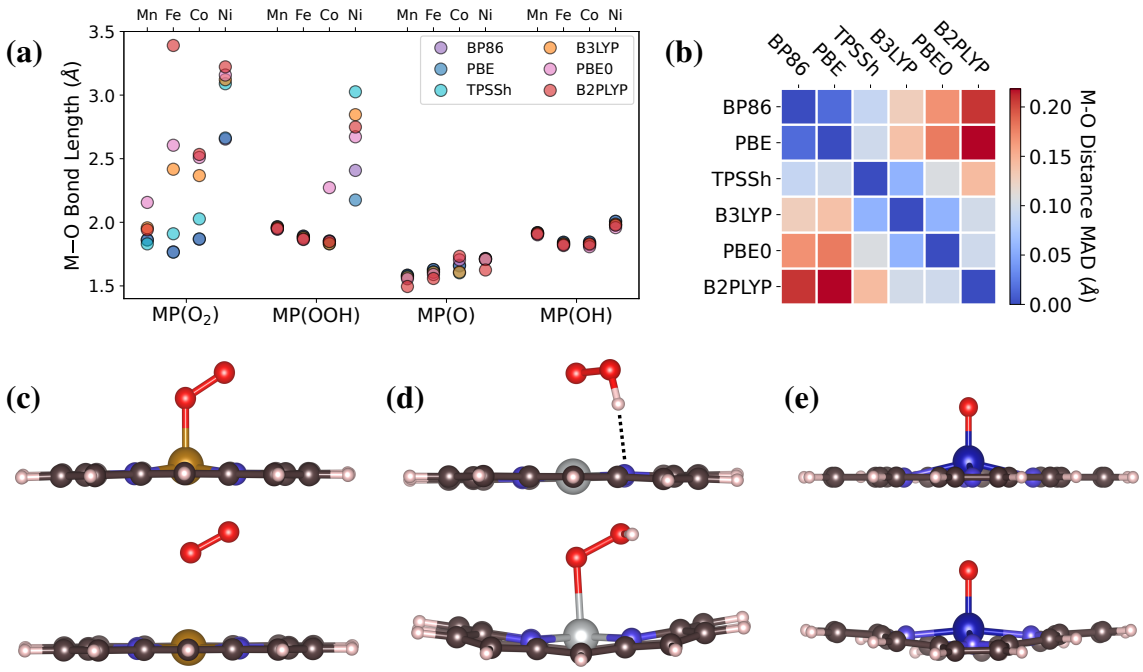

Figure 5: Dependence of geometries on employed density functional. Panel **(a)** shows the metal-oxygen bond lengths for all oxygen-containing intermediates computed with each functional. Panel **(b)** shows the Mean Absolute Deviation (MAD) of metal-oxygen bonds for pairs of functionals across all metalloporphyrin geometries and all tested multiplicities. Panel **(c)** shows BP86 (top) and PBE0 (bottom) structures of $FeP(O_2)$ with multiplicity 1. Panel **(d)** shows B3LYP (top) and PBE (bottom) structures of NiP(OOH) with multiplicity 2. Panel **(e)** shows B3LYP (top) and PBE0 (bottom) structures of CoP(O) with multiplicity 4.

remain small (< 0.1 *Å* and < 5 kcal/mol, respectively) across all intermediates for a given functional. This indicates that the relative energies of intermediates, and therefore computed catalyst activities, are only minimally affected by the functional used for geometry optimization. However, there are some notable exceptions. The weak-binding intermediates $FeP(O_2)$, $CoP(O_2)$, and NiP(OOH) all show intermediate to large RMSDs and large energy differences for at least one functional. These results suggest that caution should be taken when determining the structures of weak binding MP intermediates, though we note that this is rarely an issue for the determination of overpotentials since the dioxygen intermediate is not required for these.

These results also provide a strong warning against the use of double-hybrid functionals for metalloporphyrins. B2PLYP shows very large relative energies for MnP(O), FeP(O), CoP(OOH) and NiP(OH) despite these intermediates having small RMSDs. All of these complexes showed

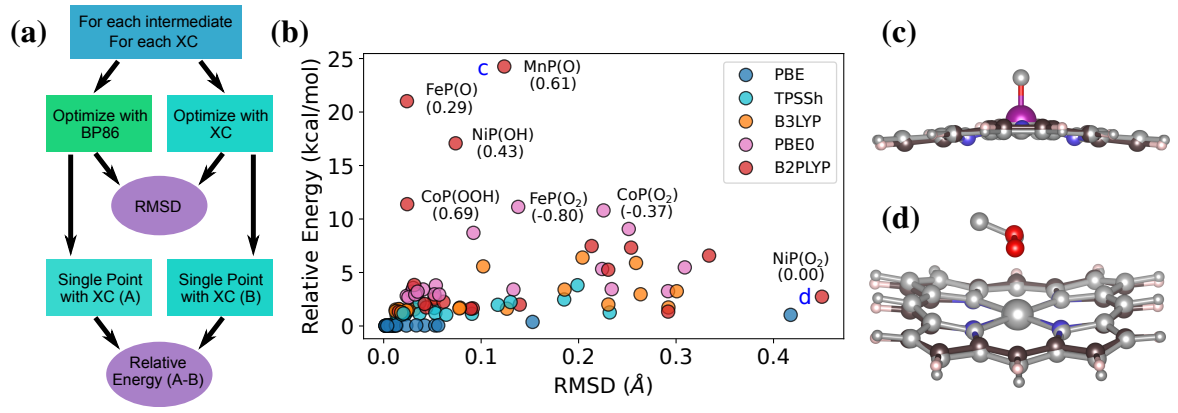

Figure 6: Comparison of geometries optimized by BP86 and other functionals. **(a)** Outline of the procedure for calculating the RMSD values and relative energies of BP86 geometries shown in Panel (b). **(b)** Energies of BP86-optimized geometries relative to the reoptimized geometries are plotted against the RMSD for these same two geometries for the ground states of all intermediates. Structures with large RMSD and relative energies have been labeled, with the change in spin contamination between the BP86 geometry and the reoptimized one ($\langle S^2 \rangle_{BP86} - \langle S^2 \rangle_{XC}$) indicated in brackets. **(c)** Overlay of the MnP(O) optimized at the BP86 (grey) and B2PLYP (color) levels. **(d)** Overlay of NiP(O_2) optimized at the BP86 (grey) and B2PLYP (color) levels.

large increases in $\langle S^2 \rangle$, and hence spin-contamination, at the BP86 geometry compared to the B2PLYP one, and the geometries of FeP(O) and NiP(OH) would not converge using B2PLYP. It is well established that the Møller-Plesset perturbation series converges more slowly for spin-contaminated references[69,70] and that MP2 fails dramatically in frequency calculations for geometries where spin contamination changes rapidly as a function of nuclear coordinates.[71] However, other work has argued that double-hybrids benefit from a cancellation of the energetic effects of spin contamination at the Hartree-Fock and MP2 levels.[72] Our results, including comparison with resricted open-shell calculations (Figure S3) suggest that the studied metalloporphyrins do not always benefit from this cancellation of errors, perhaps because of the accessibility of multiple low-lying spin states that can contaminate the wavefunction. Furthermore, recent investigations have shown that even absent spin contamination, double-hybrids may be unreliable for ligands capable of both σ-donation and π backbonding.[73] Given these drawbacks and the lack of notable improvement over single hybrid functionals, we recommend against the use of double-hybrid functionals for metalloporphyrin and related systems without careful comparison against reference data.

3.5 Variation in ΔG^0_{ORR} and Empirical O_2 Corrections

Finally, it is worth considering the extent to which the treatment of the gas-phase species H_2, H_2O, and O_2 by different functionals impacts calculated reaction pathways. To this end, we examine how the free energy of the overall 4-electron reduction of O_2 to water (eq S7) depends on the functional used and how empirical corrections to O_2 interact with this dependence.

The DFT reaction free energies were compared to the experimental value of -4.92 eV (-113.5 kcal/mol). Additionally, the atomization enthalpies of the involved molecules were calculated to pinpoint sources of error in the overall free energies. Table 3 shows these values and their errors, referenced against experimental results. Experimental values of $\Delta H^0_{at}(O_2)$ (118.876 kcal/mol) and $\Delta H^0_{at}(H_2)$ (104.154 kcal/mol) were taken from Luo[74] and $\Delta H^0_{at}(H_2O)$ (221.558 kcal/mol) from the NIST CCCBDB Database.[75]

Table 3: Theoretical oxygen reduction free energy and relevant atomization enthalpies in kcal/mol.[a]

Method	$\Delta G(ORR)$	$\Delta H^0_{at}(O_2)$	$\Delta H^0_{at}(H_2)$	$\Delta H^0_{at}(H_2O)$
BP86	-101.2 (12.2)	138.5 (19.6)	106.5 (2.3)	227.5 (5.9)
PBE	-103.0 (10.5)	142.3 (23.4)	99.5 (-4.6)	223.3 (1.8)
TPSSh	-95.2 (18.3)	119.1 (0.2)	107.4 (3.2)	215.7 (-5.9)
B3LYP	-104.7 (8.8)	121.6 (2.7)	105.1 (0.9)	219.4 (-2.2)
PBE0	-107.8 (5.6)	122.9 (4.0)	99.1 (-5.0)	215.6 (-5.9)
B2PLYP	-108.1 (5.4)	122.0 (3.1)	103.4 (-0.8)	219.5 (-2.0)
CCSD(T)	-113.6 (-0.1)	117.8 (-1.1)	103.9 (-0.3)	220.7 (-0.8)

[a] Values in parentheses indicate errors relative to the reference values.

Moving from lower to higher runs of Jacob's ladder (top to bottom in Table 3) generally improves the predicted free energy of the ORR (the poor performance of TPSSh is a notable exception to this trend). Nevertheless, none of the tested functionals approach chemical accuracy (error ≤ 1 kcal/mol). Thus, semi-empirical corrections are important for the ORR. The poor treatment of O_2 atomization energies[76] and adsorption energies[77] relative to H_2 or H_2O by GGA functionals is typically used to justify an empirical correction to O_2 alone in order to bring calculated G^0_{ORR} values in line with experiment.[23,28] However, the errors associated with H_2 and H_2O have been shown to be

important for some GGA functionals.[78,79] Another recent study of the 2-electron ORR showed that for both GGA and hybrid functionals, O_2-only corrections were insufficient in the face of similar order-of-magnitude errors in gas phase H_2O_2.[49] As a result, it is important to consider any similar magnitude gas-phase errors before applying an O_2-only correction.

In Table 3, the atomization energy of O_2 shows the expected large error for GGA functionals but a significantly reduced error for hybrid functionals and B2PLYP. For these higher-level functionals, these errors are of similar magnitude to those in the H_2 and H_2O atomization energies, leading us to believe that hybrid functionals treat all of these species with a comparable level of accuracy. Some caution is advised when using the accuracy of atomization energies to draw conclusions about a functional's accuracy for thermochemistry, as these do not correlate well in general.[80] For GGA functionals specifically, errors in atomization energies often derive more from a poor treatment of the spin polarized single atoms than from the treatment of molecules.[81] Bearing this in mind, we still believe that the uniformly small errors in atomization energies across all species for (double-) hybrid functionals indicates that the error associated with the O_2 molecule can no longer be considered *a priori* to be an order of magnitude worse than H_2O and H_2. This assertion is supported by recent work on $H_xN_yO_z$ molecules, which concluded that unlike with GGA functionals, corrections for O_2 were were unnecessary to produce accurate formation enthalpies when using B3LYP and PBE0.[82]

It thus seems likely that for (double-) hybrid functionals, residual errors in ΔG^0_{ORR} have more to do with the incomplete cancellation of relatively small errors spread across all three species in the reaction than with a single error concentrated on O_2. Atomization energy errors in Table 3 suggest that lack of error cancellation is particularly to blame for the poor reaction free energy of TPSSh, while the relatively good free energy of PBE0 results from some fortuitous cancellation. If this is the case, merely shifting the O_2 free energy to correct the overall reaction free energy means that this O_2 energy absorbs the errors associated with H_2 and H_2O, introducing a bias that depends on the distribution of these errors, which is not systematic across functionals (Table 3).

Thus, while the proposal of an alternative gas-phase correction scheme is outside the scope of

this work, we do think that the existing O_2 correction scheme does introduce a source of variability associated with the chosen functional. For hybrid functionals, this variability should be small in most cases, but perhaps not insignificant in light of the otherwise high accuracy of these functionals. Improved corrections may therefore be necessary to match the high performance of modern functionals without introducing spurious errors.

4 Conclusions

In the present study, we evaluated the dependence of the theoretical activities and linear scaling relationships of metalloporphyrin catalysts on the particular functional used. Comparisons of the relative energies of intermediates with DLPNO-CCSD(T) showed that GGAs tended to overstabilize axial oxygen-containing ligands, double-hybrids understabilized them, and single hybrids stabilized them according to the amount of exact exchange in the functional. For the present systems, B3LYP, with its 20% exchange, produced the best accuracy while also minimizing bias toward over- or under-binding.

Breaking down the differences between functionals, we found that ground state spin state predictions were quite dependent on the presence of exact exchange in a functional and could have a significant impact on theoretical catalyst activities if not properly assigned. Pooling the predictions of functionals with different amounts of exchange, however, almost always generated an assignment in line with experiment and DLPNO-CCSD(T). On the other hand, geometries were generally resilient to the choice of functional. Exceptions included the metal-oxygen bonds of weakly bound intermediates and some striking difficulties with geometry convergence and poor energies for spin-contaminated wavefunctions when using B2PLYP, which highlight the potential pitfalls of using double-hybrid functionals for these systems. Finally, we believe the commonly used empirical O_2 correction could be an additional source of variation among functionals due to the different accuracy of GGAs and hybrids in treating O_2. This correction should be reassessed as hybrid functionals become more commonplace in theoretical catalysis studies.

The density functional dependence of catalyst activities and linear scaling relationships is important for the rational design of ORR catalysts. The binding strength of intermediates dictates the thermodynamically limiting electron transfer step and indicates whether key binding interactions need to be strengthened or weakened to increase catalyst activity. Thus, for catalysts with intermediate binding strengths, the choice of functional can have an immediate impact on catalyst design choices. We hope that the present work can guide the informed use of functionals for the study of porphyrins and other M-N-C catalysts for the ORR. Hybrid functionals, with the occasional use of DLPNO-CCSD(T) for reference and validation, represent a promising path forward.

5 Supporting Information

Additional computational details, methods, and materials, including volcano plot construction, benchmarking of DLPNO-CCSD(T), DLPNO-CCSD(T) spin splittings, and characterization of geometries and spin contamination (PDF).

Energies and geometry characterization for all structures (XLSX)

Acknowledgement

We acknowledge the support of the Natural Sciences and Engineering Research Council of Canada (NSERC). This research was enabled in part by support provided by WestGrid (www.westgrid.ca) and Compute Canada (www.computecanada.ca).

References

(1) He, Y.; Liu, S.; Priest, C.; Shi, Q.; Wu, G. Atomically dispersed metal-nitrogen-carbon catalysts for fuel cells: Advances in catalyst design, electrode performance, and durability improvement. *Chemical Society Reviews* **2020**, *49*, 3484–3524.

(2) Kulkarni, A.; Siahrostami, S.; Patel, A.; Nørskov, J. K. Understanding Catalytic Activity Trends in the Oxygen Reduction Reaction. *Chemical Reviews* **2018**, *118*, 2302–2312.

(3) Montoya, J. H.; Seitz, L. C.; Chakthranont, P.; Vojvodic, A.; Jaramillo, T. F.; Nørskov, J. K. Materials for solar fuels and chemicals. *Nature Materials* **2016**, *16*, 70–81.

(4) Busch, M.; Halck, N. B.; Kramm, U. I.; Siahrostami, S.; Krtil, P.; Rossmeisl, J. Beyond the top of the volcano? – A unified approach to electrocatalytic oxygen reduction and oxygen evolution. *Nano Energy* **2016**, *29*, 126–135.

(5) Sours, T.; Patel, A.; Nørskov, J.; Siahrostami, S.; Kulkarni, A. Circumventing Scaling Relations in Oxygen Electrochemistry Using Metal–Organic Frameworks. *The Journal of Physical Chemistry Letters* **2020**, *11*, 10029–10036.

(6) Chung, H. T.; Cullen, D. A.; Higgins, D.; Sneed, B. T.; Holby, E. F.; More, K. L.; Zelenay, P. Direct atomic-level insight into the active sites of a high-performance PGM-free ORR catalyst. *Science* **2017**, *357*, 479–484.

(7) Baran, J. D.; Grönbeck, H.; Hellman, A. Analysis of Porphyrines as Catalysts for Electrochemical Reduction of O2 and Oxidation of H2O. *Journal of the American Chemical Society* **2014**, *136*, 1320–1326.

(8) Lv, B.; Li, X.; Guo, K.; Ma, J.; Wang, Y.; Lei, H.; Wang, F.; Jin, X.; Zhang, Q.; Zhang, W.; Long, R.; Xiong, Y.; Apfel, U.; Cao, R. Controlling Oxygen Reduction Selectivity through Steric Effects: Electrocatalytic Two-Electron and Four-Electron Oxygen Reduction with Cobalt Porphyrin Atropisomers. *Angewandte Chemie International Edition* **2021**, *60*, 12742–12746.

(9) Drosou, M.; Mitsopoulou, C. A.; Pantazis, D. A. Reconciling Local Coupled Cluster with Multireference Approaches for Transition Metal Spin-State Energetics. *Journal of Chemical Theory and Computation* **2022**, *18*, 3538–3548.

(10) Radoń, M.; Pierloot, K. Binding of CO, NO, and O_2 to Heme by Density Functional and Multireference ab Initio Calculations. *The Journal of Physical Chemistry A* **2008**, *112*, 11824–11832.

(11) Phung, Q. M.; Pierloot, K. The dioxygen adducts of iron and manganese porphyrins: electronic structure and binding energy. *Physical Chemistry Chemical Physics* **2018**, *20*, 17009–17019.

(12) Busch, M.; Fabrizio, A.; Luber, S.; Hutter, J.; Corminboeuf, C. Exploring the Limitation of Molecular Water Oxidation Catalysts. *The Journal of Physical Chemistry C* **2018**, *122*, 12404–12412.

(13) Patel, A. M.; Ringe, S.; Siahrostami, S.; Bajdich, M.; Nørskov, J. K.; Kulkarni, A. R. Theoretical Approaches to Describing the Oxygen Reduction Reaction Activity of Single-Atom Catalysts. *The Journal of Physical Chemistry C* **2018**, *122*, 29307–29318.

(14) Jiang, W.; Laury, M. L.; Powell, M.; Wilson, A. K. Comparative Study of Single and Double Hybrid Density Functionals for the Prediction of 3d Transition Metal Thermochemistry. *Journal of Chemical Theory and Computation* **2012**, *8*, 4102–4111.

(15) Moltved, K. A.; Kepp, K. P. Performance of Density Functional Theory for Transition Metal Oxygen Bonds. *ChemPhysChem* **2019**, *20*, 3210–3220.

(16) Maurer, L. R.; Bursch, M.; Grimme, S.; Hansen, A. Assessing Density Functional Theory for Chemically Relevant Open-Shell Transition Metal Reactions. *Journal of Chemical Theory and Computation* **2021**, *17*, 6134–6151.

(17) Pegis, M. L.; Wise, C. F.; Martin, D. J.; Mayer, J. M. Oxygen Reduction by Homogeneous Molecular Catalysts and Electrocatalysts. *Chemical Reviews* **2018**, *118*, 2340–2391.

(18) Govindarajan, N.; Koper, M. T. M.; Meijer, E. J.; Calle-Vallejo, F. Outlining the Scaling-Based and Scaling-Free Optimization of Electrocatalysts. *ACS Catalysis* **2019**, *9*, 4218–4225.

(19) Kaur, H.; Goel, N. Tailoring the cobalt porphyrin for minimal overpotential in the electrochemical oxygen evolution/reduction reactions: A density functional study. *International Journal of Hydrogen Energy* **2023**, *48*, 31720–31733.

(20) Dung, T. P.; Chihaia, V.; Son, D. N. Effects of functional groups in iron porphyrin on the mechanism and activity of oxygen reduction reaction. *RSC Advances* **2023**, *13*, 8523–8534.

(21) Elghamry, I.; Alablan, A. S.; Alkhalifah, M. A.; Abdelsalam, M. E. High-Performance Organometallic Catalyst Based on Nickel Porphyrin/Carbon Fibre for the Oxygen Reduction Reaction. *Journal of The Electrochemical Society* **2021**, *168*, 016510.

(22) Pegis, M. L.; McKeown, B. A.; Kumar, N.; Lang, K.; Wasylenko, D. J.; Zhang, X. P.; Raugei, S.; Mayer, J. M. Homogenous Electrocatalytic Oxygen Reduction Rates Correlate with Reaction Overpotential in Acidic Organic Solutions. *ACS Central Science* **2016**, *2*, 850–856.

(23) Nørskov, J. K.; Rossmeisl, J.; Logadottir, A.; Lindqvist, L.; Kitchin, J. R.; Bligaard, T.; Jónsson, H. Origin of the Overpotential for Oxygen Reduction at a Fuel-Cell Cathode. *The Journal of Physical Chemistry B* **2004**, *108*, 17886–17892.

(24) Calle-Vallejo, F.; Martínez, J. I.; Rossmeisl, J. Density functional studies of functionalized graphitic materials with late transition metals for oxygen reduction reactions. *Physical Chemistry Chemical Physics* **2011**, *13*, 15639.

(25) Calle-Vallejo, F.; Martínez, J.; García-Lastra, J.; Abad, E.; Koper, M. Oxygen reduction and evolution at single-metal active sites: Comparison between functionalized graphitic materials and protoporphyrins. *Surface Science* **2013**, *607*, 47–53.

(26) Calle-Vallejo, F.; Krabbe, A.; García-Lastra, J. M. How covalence breaks adsorption-energy scaling relations and solvation restores them. *Chemical Science* **2017**, *8*, 124–130.

(27) Ma, R.; Lin, G.; Zhou, Y.; Liu, Q.; Zhang, T.; Shan, G.; Yang, M.; Wang, J. A review of oxygen reduction mechanisms for metal-free carbon-based electrocatalysts. *npj Computational Materials* **2019**, *5*.

(28) Sargeant, E.; Illas, F.; Rodríguez, P.; Calle-Vallejo, F. Importance of the gas-phase error correction for O2 when using DFT to model the oxygen reduction and evolution reactions. *Journal of Electroanalytical Chemistry* **2021**, *896*, 115178.

(29) Conway, B. E., Bockris, J. O., Yeager, E., Khan, S. U. M., White, R. E., Eds. *Comprehensive Treatise of Electrochemistry*; Springer New York, NY, 1983; Vol. 7.

(30) Bratsch, S. G. Standard Electrode Potentials and Temperature Coefficients in Water at 298.15 K. *Journal of Physical and Chemical Reference Data* **1989**, *18*, 1–21.

(31) Grimme, S.; Antony, J.; Ehrlich, S.; Krieg, H. A consistent and accurate ab initio parametrization of density functional dispersion correction (DFT-D) for the 94 elements H-Pu. *J. Chem. Phys.* **2010**, *132*, 154104.

(32) Grimme, S.; Ehrlich, S.; Goerigk, L. Effect of the damping function in dispersion corrected density functional theory. *J. Comput. Chem.* **2011**, *32*, 1456–1465.

(33) Perdew, J. P. Jacob's ladder of density functional approximations for the exchange-correlation energy. AIP Conference Proceedings. 2001.

(34) Becke, A. D. Density-functional exchange-energy approximation with correct asymptotic behavior. *Physical Review A* **1988**, *38*, 3098–3100.

(35) Perdew, J. P. Density-functional approximation for the correlation energy of the inhomogeneous electron gas. *Physical Review B* **1986**, *33*, 8822–8824.

(36) Perdew, J. P.; Burke, K.; Ernzerhof, M. Generalized Gradient Approximation Made Simple. *Physical Review Letters* **1996**, *77*, 3865–3868.

(37) Staroverov, V. N.; Scuseria, G. E.; Tao, J.; Perdew, J. P. Comparative assessment of a new nonempirical density functional: Molecules and hydrogen-bonded complexes. *The Journal of Chemical Physics* **2003**, *119*, 12129–12137.

(38) Becke, A. D. Density-functional thermochemistry. III. The role of exact exchange. *The Journal of Chemical Physics* **1993**, *98*, 5648–5652.

(39) Adamo, C.; Barone, V. Toward reliable density functional methods without adjustable parameters: The PBE0 model. *The Journal of Chemical Physics* **1999**, *110*, 6158–6170.

(40) Grimme, S. Semiempirical hybrid density functional with perturbative second-order correlation. *Journal of Chemical Physics* **2006**, *124*, 034108.

(41) Goerigk, L.; Grimme, S. Efficient and Accurate Double-Hybrid-Meta-GGA Density Functionals—Evaluation with the Extended GMTKN30 Database for General Main Group Thermochemistry, Kinetics, and Noncovalent Interactions. *Journal of Chemical Theory and Computation* **2010**, *7*, 291–309.

(42) Bauernschmitt, R.; Ahlrichs, R. Stability analysis for solutions of the closed shell Kohn–Sham equation. *The Journal of Chemical Physics* **1996**, *104*, 9047–9052.

(43) Guo, Y.; Riplinger, C.; Becker, U.; Liakos, D. G.; Minenkov, Y.; Cavallo, L.; Neese, F. Communication: An improved linear scaling perturbative triples correction for the domain based local pair-natural orbital based singles and doubles coupled cluster method [DLPNO-CCSD(T)]. *The Journal of Chemical Physics* **2018**, *148*.

(44) Guo, Y.; Riplinger, C.; Liakos, D. G.; Becker, U.; Saitow, M.; Neese, F. Linear scaling perturbative triples correction approximations for open-shell domain-based local pair natural orbital coupled cluster singles and doubles theory [DLPNO-CCSD(T/T)]. *The Journal of Chemical Physics* **2020**, *152*.

(45) Neese, F.; Valeev, E. F. Revisiting the Atomic Natural Orbital Approach for Basis Sets: Robust Systematic Basis Sets for Explicitly Correlated and Conventional Correlated *ab initio* Methods? *Journal of Chemical Theory and Computation* **2010**, *7*, 33–43.

(46) Altun, A.; Neese, F.; Bistoni, G. Extrapolation to the Limit of a Complete Pair Natural Orbital Space in Local Coupled-Cluster Calculations. *Journal of Chemical Theory and Computation* **2020**, *16*, 6142–6149.

(47) Calle-Vallejo, F.; Martínez, J. I.; García-Lastra, J. M.; Rossmeisl, J.; Koper, M. T. M. Physical and Chemical Nature of the Scaling Relations between Adsorption Energies of Atoms on Metal Surfaces. *Physical Review Letters* **2012**, *108*.

(48) Dohm, S.; Hansen, A.; Steinmetz, M.; Grimme, S.; Checinski, M. P. Comprehensive Thermochemical Benchmark Set of Realistic Closed-Shell Metal Organic Reactions. *Journal of Chemical Theory and Computation* **2018**, *14*, 2596–2608.

(49) Almeida, M. O.; Kolb, M. J.; Lanza, M. R. V.; Illas, F.; Calle-Vallejo, F. Gas-Phase Errors Affect DFT-Based Electrocatalysis Models of Oxygen Reduction to Hydrogen Peroxide. *ChemElectroChem* **2022**, *9*.

(50) Shee, J.; Loipersberger, M.; Rettig, A.; Lee, J.; Head-Gordon, M. Regularized Second-Order Møller–Plesset Theory: A More Accurate Alternative to Conventional MP2 for Noncovalent Interactions and Transition Metal Thermochemistry for the Same Computational Cost. *The Journal of Physical Chemistry Letters* **2021**, *12*, 12084–12097.

(51) Reiher, M.; Salomon, O.; Hess, B. A. Reparameterization of hybrid functionals based on energy differences of states of different multiplicity. *Theoretical Chemistry Accounts: Theory, Computation, and Modeling (Theoretica Chimica Acta)* **2001**, *107*, 48–55.

(52) Fouqueau, A.; Casida, M. E.; Daku, L. M. L.; Hauser, A.; Neese, F. Comparison of density functionals for energy and structural differences between the high- [5T2g:(t2g)4(eg)2] and

low- [1A1g:(t2g)6(eg)] spin states of iron(II) coordination compounds. II. More functionals and the hexaminoferrous cation, [Fe(NH3)6]2+. *The Journal of Chemical Physics* **2005**, *122*.

(53) Neese, F. Prediction of molecular properties and molecular spectroscopy with density functional theory: From fundamental theory to exchange-coupling. *Coordination Chemistry Reviews* **2009**, *253*, 526–563.

(54) Collman, J. P.; Hoard, J. L.; Kim, N.; Lang, G.; Reed, C. A. Synthesis, stereochemistry, and structure-related properties of .alpha., .beta., .gamma., .delta.-tetraphenylporphinatoiron(II). *Journal of the American Chemical Society* **1975**, *97*, 2676–2681.

(55) Goff, H.; La Mar, G. N.; Reed, C. A. Nuclear magnetic resonance investigation of magnetic and electronic properties of "intermediate spin" ferrous porphyrin complexes. *Journal of the American Chemical Society* **1977**, *99*, 3641–3646.

(56) Kirner, J. F.; Reed, C. A.; Scheidt, W. R. Stereochemistry of manganese porphyrins. 2. The toluene solvate of .alpha., .beta., .gamma., .delta.-tetraphenylporphinatomanganese(II) at 20 and -175.degree.C. *Journal of the American Chemical Society* **1977**, *99*, 1093–1101.

(57) Madura, P.; Scheidt, W. R. Stereochemistry of low-spin cobalt porphyrins. 8. .alpha., .beta., .gamma., .delta.-Tetraphenylporphinatocobalt(II). *Inorganic Chemistry* **1976**, *15*, 3182–3184.

(58) Pauling, L.; Coryell, C. D. The Magnetic Properties and Structure of the Hemochromogens and Related Substances. *Proceedings of the National Academy of Sciences* **1936**, *22*, 159–163.

(59) Smith, K. *Porphyrins and Metalloporphyrins: A New Edition Based on the Original Volume by J. E. Falk*; BBA Library; Elsevier Scientific Publishing Company, 1975.

(60) Gutzeit, F.; Dommaschk, M.; Levin, N.; Buchholz, A.; Schaub, E.; Plass, W.; Näther, C.;

Herges, R. Structure and Properties of a Five-Coordinate Nickel(II) Porphyrin. *Inorganic Chemistry* **2019**, *58*, 12542–12546.

(61) Hoffman, B. M.; Szymanski, T.; Brown, T. G.; Basolo, F. The dioxygen adducts of several manganese(II) porphyrins. Electron paramagnetic resonance studies. *Journal of the American Chemical Society* **1978**, *100*, 7253–7259.

(62) Gallagher, A. T.; Lee, J. Y.; Kathiresan, V.; Anderson, J. S.; Hoffman, B. M.; Harris, T. D. A structurally-characterized peroxomanganese(¡scp¿iv¡/scp¿) porphyrin from reversible O2 binding within a metal–organic framework. *Chemical Science* **2018**, *9*, 1596–1603.

(63) Latos-Grazynski, L.; Cheng, R. J.; La Mar, G. N.; Balch, A. L. Oxygenation patterns for substituted meso-tetraphenylporphyrin complexes of iron(II). Spectroscopic detection of dioxygen complexes in the absence of amines. *Journal of the American Chemical Society* **1982**, *104*, 5992–6000.

(64) Anderson, J. S.; Gallagher, A. T.; Mason, J. A.; Harris, T. D. A Five-Coordinate Heme Dioxygen Adduct Isolated within a Metal–Organic Framework. *Journal of the American Chemical Society* **2014**, *136*, 16489–16492.

(65) Gallagher, A. T.; Kelty, M. L.; Park, J. G.; Anderson, J. S.; Mason, J. A.; Walsh, J. P. S.; Collins, S. L.; Harris, T. D. Dioxygen binding at a four-coordinate cobaltous porphyrin site in a metal–organic framework: structural, EPR, and O2adsorption analysis. *Inorganic Chemistry Frontiers* **2016**, *3*, 536–540.

(66) Pierloot, K.; Phung, Q. M.; Domingo, A. Spin State Energetics in First-Row Transition Metal Complexes: Contribution of (3s3p) Correlation and Its Description by Second-Order Perturbation Theory. *Journal of Chemical Theory and Computation* **2017**, *13*, 537–553.

(67) Phung, Q. M.; Feldt, M.; Harvey, J. N.; Pierloot, K. Toward Highly Accurate Spin State Energetics in First-Row Transition Metal Complexes: A Combined CASPT2/CC Approach. *Journal of Chemical Theory and Computation* **2018**, *14*, 2446–2455.

(68) Ovalle, S.; Malardier-Jugroot, C. Choice of functional for iron porphyrin density functional theory studies: Geometry, spin-state, and binding energy analysis. *Computational and Theoretical Chemistry* **2022**, *1213*, 113726.

(69) Handy, N. C.; Knowles, P. J.; Somasundram, K. On the convergence of the Møller-Plesset perturbation series. *Theoretica Chimica Acta* **1985**, *68*, 87–100.

(70) Gill, P. M. W.; Pople, J. A.; Radom, L.; Nobes, R. H. Why does unrestricted Møller–Plesset perturbation theory converge so slowly for spin-contaminated wave functions? *The Journal of Chemical Physics* **1988**, *89*, 7307–7314.

(71) Jensen, F. A remarkable large effect of spin contamination on calculated vibrational frequencies. *Chemical Physics Letters* **1990**, *169*, 519–528.

(72) Menon, A. S.; Radom, L. Consequences of Spin Contamination in Unrestricted Calculations on Open-Shell Species: Effect of Hartree-Fock and Møller-Plesset Contributions in Hybrid and Double-Hybrid Density Functional Theory Approaches. *The Journal of Physical Chemistry A* **2008**, *112*, 13225–13230.

(73) Shee, J.; Loipersberger, M.; Hait, D.; Lee, J.; Head-Gordon, M. Revealing the nature of electron correlation in transition metal complexes with symmetry breaking and chemical intuition. *The Journal of Chemical Physics* **2021**, *154*.

(74) Luo, Y.-R. *Comprehensive Handbook of Chemical Bond Energies*; CRC Press, 2007.

(75) NIST Computational Chemistry Comparison and Benchmark Database. 2022; NIST Standard Reference Database Number 101.

(76) Kurth, S.; Perdew, J. P.; Blaha, P. Molecular and solid-state tests of density functional approximations: LSD, GGAs, and meta-GGAs. *International Journal of Quantum Chemistry* **1999**, *75*, 889–909.

(77) Wellendorff, J.; Silbaugh, T. L.; Garcia-Pintos, D.; Nørskov, J. K.; Bligaard, T.; Studt, F.; Campbell, C. T. A benchmark database for adsorption bond energies to transition metal surfaces and comparison to selected DFT functionals. *Surface Science* **2015**, *640*, 36–44.

(78) Studt, F.; Behrens, M.; Kunkes, E. L.; Thomas, N.; Zander, S.; Tarasov, A.; Schumann, J.; Frei, E.; Varley, J. B.; Abild-Pedersen, F.; Nørskov, J. K.; Schlögl, R. The Mechanism of CO and CO2 Hydrogenation to Methanol over Cu-Based Catalysts. *ChemCatChem* **2015**, *7*, 1105–1111.

(79) Christensen, R.; Hansen, H. A.; Dickens, C. F.; Nørskov, J. K.; Vegge, T. Functional Independent Scaling Relation for ORR/OER Catalysts. *The Journal of Physical Chemistry C* **2016**, *120*, 24910–24916.

(80) Margraf, J. T.; Ranasinghe, D. S.; Bartlett, R. J. Automatic generation of reaction energy databases from highly accurate atomization energy benchmark sets. *Physical Chemistry Chemical Physics* **2017**, *19*, 9798–9805.

(81) Perdew, J. P.; Sun, J.; Ruzsinszky, A.; Mezei, P. D.; Csonka, G. I. Why Density Functionals Should Not Be Judged Primarily by Atomization Energies. *Periodica Polytechnica Chemical Engineering* **2016**, *60*, 2–7.

(82) Urrego-Ortiz, R.; Builes, S.; Calle-Vallejo, F. Impact of Intrinsic Density Functional Theory Errors on the Predictive Power of Nitrogen Cycle Electrocatalysis Models. *ACS Catalysis* **2022**, *12*, 4784–4791.

TOC Graphic